Neurobiology of Disease

An Epilepsy-Associated SV2A Mutation Disrupts Synaptotagmin-1 Expression and Activity-Dependent Trafficking

Callista B. Harper,[1,2,3] Christopher Small,[4] Elizabeth C. Davenport,[1,2,3] Darryl W. Low,[1,2] Karen J. Smillie,[1,2] Ramón Martínez-Mármol,[4] Frédéric A. Meunier,[4] and Michael A. Cousin[1,2,3]

[1]Centre for Discovery Brain Sciences, Hugh Robson Building, University of Edinburgh, Edinburgh, EH8 9XD, United Kingdom, [2]Muir Maxwell Epilepsy Centre, University of Edinburgh, Edinburgh EH8 9XD, United Kingdom, [3]Simons Initiative for the Developing Brain, University of Edinburgh, Edinburgh EH8 9XD, United Kingdom, and [4]Clem Jones Centre for Ageing Dementia Research, Queensland Brain Institute, The University of Queensland, Brisbane, Queensland QLD 4072, Australia

The epilepsy-linked gene *SV2A*, has a number of potential roles in the synaptic vesicle (SV) life cycle. However, how loss of SV2A function translates into presynaptic dysfunction and ultimately seizure activity is still undetermined. In this study, we examined whether the first SV2A mutation identified in human disease (R383Q) could provide information regarding which SV2A-dependent events are critical in the translation to epilepsy. We utilized a molecular replacement strategy in which exogenous SV2A was expressed in mouse neuronal cultures of either sex, which had been depleted of endogenous SV2A to mimic the homozygous human condition. We found that the R383Q mutation resulted in a mislocalization of SV2A from SVs to the plasma membrane, but had no effect on its activity-dependent trafficking. This SV2A mutant displayed reduced mobility when stranded on the plasma membrane and reduced binding to its interaction partner synaptotagmin-1 (Syt1). Furthermore, the R383Q mutant failed to rescue reduced expression and dysfunctional activity-dependent trafficking of Syt1 in the absence of endogenous SV2A. This suggests that the inability to control Syt1 expression and trafficking at the presynapse may be key in the transition from loss of SV2A function to seizure activity.

Key words: endocytosis; epilepsy; exocytosis; SV2A; synaptotagmin; vesicle

---

Significance Statement

SV2A is a synaptic vesicle (SV) protein, the absence or dysfunction of which is linked to epilepsy. However, the series of molecular events that result in this neurological disorder is still undetermined. We demonstrate here that the first human mutation in SV2A identified in an individual with epilepsy displays reduced binding to synaptotagmin-1 (Syt1), an SV protein essential for synchronous neurotransmitter release. Furthermore, this mutant cannot correct alterations in both Syt1 expression and trafficking when expressed in the absence of endogenous SV2A (to mimic the homozygous human condition). This suggests that the inability to control Syt1 expression and trafficking may be key in the transition from loss of SV2A function to seizure activity.

Introduction

SV2A is a multitransmembrane synaptic vesicle (SV) protein, the dysfunction of which is linked to epilepsy via a series of independent observations (Mendoza-Torreblanca et al., 2013;

Ciruelas et al., 2019). First, SV2A is the binding target of the leading anti-epileptic drug levetiracetam (Lynch et al., 2004). Second, deletion of the *Sv2a* gene in mice results in severe seizures and lethality after two to three weeks (Crowder et al., 1999; Janz et al., 1999). Third, rats harboring a missense mutation in SV2A (L174Q) display increased seizure susceptibility (Tokudome

et al., 2016a,b). Finally, a homozygous mutation in the *SV2A* gene in an individual with intractable epilepsy (R383Q) was identified (Serajee and Huq, 2015). Therefore, evidence is accumulating that loss of SV2A function plays a key role in precipitating seizure activity. However, it is still unclear how SV2A dysfunction translates into epilepsy.

SV2A is proposed to perform multiple roles at the presynapse (Mendoza-Torreblanca et al., 2013; Ciruelas et al., 2019). One role is as an intrinsic trafficking partner (iTRAP) during SV endocytosis (Gordon and Cousin, 2016). The efficient endocytosis of SVs is essential for maintenance of neurotransmission at central nerve terminals (Chanaday et al., 2019). A series of cargo capture and clustering mechanisms ensure that SVs possess the correct complement of membrane cargo with the correct stoichiometry. SV cargos are clustered by adaptor protein complexes such as AP-2 and/or monomeric adaptor proteins such as AP180 and stonin-2 (Kelly and Owen, 2011; Koo et al., 2011, 2015; Kononenko et al., 2013). In addition, SV cargos called iTRAPs share interactions with specific SV proteins to ensure a high fidelity of retrieval during endocytosis (Yao et al., 2010; Gordon et al., 2011; Kaempf et al., 2015; Zhang et al., 2015). SV2A is an iTRAP for synaptotagmin-1 (Syt1; Gordon and Cousin, 2016), which is an essential protein for coupling calcium influx to neurotransmitter release (Geppert et al., 1994).

Loss of SV2A function, either via shRNA knock-down (Kaempf et al., 2015; Zhang et al., 2015) or genetic deletion (Yao et al., 2010) has specific effects on Syt1 function. First, the retrieval of Syt1 during endocytosis is accelerated (Kaempf et al., 2015; Zhang et al., 2015). Second, the expression of Syt1 is reduced, especially on SVs (Yao et al., 2010; Kaempf et al., 2015). SV2A interacts with the calcium-binding C2B domain of Syt1 at its cytoplasmic N terminus (Schivell et al., 1996, 2005). This interaction is triggered by the phosphorylation of a specific residue (T84) within the SV2A N terminus by casein family kinases (Pyle et al., 2000; Zhang et al., 2015). Mutagenesis of this phosphorylation site ablates Syt1 binding and renders mutant SV2A protein unable to rescue the phenotypes described above (Zhang et al., 2015).

We used a neuronal system in which endogenous SV2A was depleted and replaced with SV2A containing the R383Q mutation to mimic the homozygous human condition. We found that this mutation increased the surface localization of SV2A, and reduced its surface mobility without affecting its activity-dependent trafficking. Furthermore, the R383Q mutant displayed reduced binding to Syt1. This resulted in a lack of rescue of Syt1 expression and activity-dependent Syt1 retrieval kinetics. This association between a human SV2A mutant and a loss of control of Syt1 function suggests that the latter may be the key epileptogenic step in mammalian systems.

Materials and Methods

Materials
Unless otherwise specified, all tissue culture reagents were obtained from Invitrogen. Fetal bovine serum (FBS) was from Biosera. Papain was obtained from Worthington. Nitrocellulose membranes and molecular weight markers were from Bio-Rad. Tetrodotoxin citrate (TTX) was from Hello Bio. Primary antibodies were purchased from Abcam unless otherwise specified. All other reagents were obtained from Sigma-Aldrich.

Syt1-pHluorin was a gift from Prof. Volker Haucke (Leibniz-Institute for Molecular Pharmacology). SV2A-pHluorin, SV2A-mCerulean, and pSUPER vectors that co-express SV2A shRNA (shRNA sequence GAATTGGCTCAGCAGTATG) with either mCerulean or Syt1-pHluorin were described previously (Zhang et al., 2015). Y46A and R383Q mutations were introduced into human SV2A-pHluorin using the following primers (mutated bases underlined; Y46A forward, GCATCCAGT GATGCT<u>GC</u>TGAGGGCCATGACGAG; Y46A reverse, CTCGTCAT GGCCCT<u>C</u>AGCAGCATCACTGGATGC; R383Q forward, CATGATA CCAACATGC<u>A</u>AGCCAAAGGACATCCT; R383Q reverse, AGGATG TCCTTTGGCT<u>T</u>GCATGTTGGTATCATG). The R383Q mutation was introduced into SV2A-mCerulean using the primers: forward, CACGA CACCAACATGC<u>A</u>AGCCAAGGCCCACCCT; reverse, AGGGTGGC CCTTGGCT<u>T</u>GC<u>A</u>TGTTGGTGTCGTG. Wild-type and R383Q SV2A-mCerulean were made shRNA resistant using the primers: forward, GAGCTTGCGCAGCAATAC; reverse, GTATTGCTGCGCAAGCTC. Syt1-HA in a pCMV5 vector (DU38472) was obtained from the MRC-PPU (University of Dundee). A glutathione S-transferase (GST) fusion protein of the third cytoplasmic loop of SV2A (amino acids 356–447) was generated by amplifying DNA encoding this region from SV2A-mCerulean using the primers (forward, <u>GGATCC</u>GAGAGTCCCCG CTTCTTCCTAGAGA; reverse, <u>CTCGAG</u>TCACGTGATGCGCCGATA CTCTGGACTG) and ligating into a PGEX-4T-1 vector using the enzymes BamHI and XhoI (underlined). The R383Q mutation was introduced using identical primers to those described above for SV2A-mCerulean.

Animal maintenance
Animal work was performed in accordance with the UK Animal (Scientific Procedures) Act 1986, under Project and Personal License authority and was approved by the Animal Welfare and Ethical Review Body at the University of Edinburgh (Home Office project license 70/ 8878). Specifically, all animals were killed by schedule 1 procedures in accordance with United Kingdom Home Office Guidelines; adults were killed by cervical dislocation followed by decapitation, whereas embryos were killed by decapitation followed by destruction of the brain. Wild-type C57BL/6J mice were sourced from an in-house colony at the University of Edinburgh. All mouse colonies were housed in standard open top caging on a 14/10 h light/dark cycle (light 7 A.M. to 9 P.M.). Breeders were fed RM1 chow, whereas stock mice were maintained on RM3 chow.

For single particle tracking experiments, animal work was performed in accordance with the Australian Code and Practice for the Care and Use of Animals for Scientific Purposes and approved by the University of Queensland Animal Ethics Committee (QBI/254/16/NHMRC). Animals were housed with 12/12 h light/dark exposure (light 7 A.M. to 7 P.M.) and fed with autoclaved mouse and rat cubes (Specialty Feeds). Mice were culled by cervical dislocation and embryos were euthanized by decapitation.

Primary neuronal culture and transfection
Dissociated primary hippocampal enriched neuronal cultures were prepared from embryonic day (E)16.5–E18.5 embryos from wild-type C57/ BL6J mice of both sexes as outlined (Zhang et al., 2015; Harper et al., 2017). In brief, isolated hippocampi were digested in 10 U/ml papain in Dulbecco's PBS, washed in minimal essential medium (MEM) supplemented with 10% FBS, and triturated to single cell suspension. This cell suspension was plated at $3–5 \times 10^4$ cells on poly-D-lysine and laminin-coated 25-mm coverslips. Cells were transfected on 7–9 d *in vitro* (DIV) with Lipofectamine 2000 as per manufacturer's instructions (Gordon and Cousin, 2013).

For single particle tracking experiments, dissection and culture were performed as outlined (Joensuu et al., 2017). Briefly, embryos of both sexes were dissected in 1× HBSS, 10 mM HEPES (pH 7.3), 100 U/ml penicillin, and 100 μg/ml streptomycin. Hippocampal tissue was digested with 0.25% trypsin. Digestion was halted by addition of 5% FBS and DNase I. Cell suspension was triturated, centrifuged (120 × *g*, 7 min) and resuspended in Neurobasal Medium, 100 U/ml penicillin, 100 μg/ml streptomycin, 1× GlutaMAX supplement, 1× B27, and 5% FBS. Neurons were seeded in poly-L-lysine-coated 29-mm glass-bottom dishes (Cellvis) at a density of 1×10^5 neurons. A full media change was performed 2–4 h after seeding using culturing media (Neurobasal

Medium, 100 U/ml penicillin, 100 μg/ml streptomycin, 1× GlutaMAX supplement, and 1× B27). Cells were transfected at DIV 14–15 with Lipofectamine 2000 as per manufacturer's instructions.

Immunostaining
Cultured hippocampal neurons were washed once with PBS before fixation in 4% paraformaldehyde, quenching by 50 mM NH_4Cl and permeabilization with 0.1% v/v Triton X-100, 1% w/v bovine serum albumin (BSA) in PBS. Cultured neurons were blocked with 1% BSA in PBS before incubation with primary antibodies: chicken anti-GFP (ab13970, 1:10,000), rabbit anti-SV2A (ab13259, 1:500), and mouse anti-Syt1 (ab32942, 1:500). Rabbit anti-synaptophysin (#101002, 1:1000) was from Synaptic Systems. The cultures were washed with PBS and incubated with fluorescently conjugated secondary antibodies [goat anti-chicken Alexa Fluor 488 (Life Technologies, A11039), goat anti-rabbit Alexa Fluor 555 A21430, goat anti-mouse Alexa Fluor 647 A21235, and goat anti-rabbit Alexa Fluor 647 A21244; all 1:500). The coverslips were mounted on slides for imaging with FluorSave (Millipore).

Fluorescence imaging
Imaging was conducted on a Zeiss Axio Observer D1 or Z1/7 inverted epifluorescence microscope with a Zeiss EC Plan Neofluar 40×/1.30 oil immersion objective. Images were captured using an AxioCam 506 mono camera (Zeiss). GFP/pHluorin or mCerulean vectors were visualized at either 500- or 430-nm excitation respectively (long-pass emission filter >520 nm). Alexa Fluor 488 and 555 labeled coverslips were imaged simultaneously using double band pass excitation filters (470/27 nm + 556/25 nm) and emission filters 512/30 and 630/98 nm (Zeiss). Alexa Fluor 647 fluorescence was acquired with band pass excitation (640/30 nm) and emission filters 690/50 nm (Zeiss).

For live-cell imaging, hippocampal cultures were mounted in a Warner Instruments imaging chamber with embedded parallel platinum wires (RC-21BRFS). Cultures were stimulated with a train of 300 action potentials delivered at 10 Hz (100 mA, 1-ms pulse width) during which there was continuous perfusion of imaging buffer (119 mM NaCl, 2.5 mM KCl, 2 mM $CaCl_2$, 2 mM $MgCl_2$, 30 mM D-glucose, 25 mM HEPES; pH 7.4 supplemented with 10 μM 6-cyano-7-nitroquinoxaline-2,3-dione and 50 μM DL-2-amino-5-phosphonopentanoic acid). After 180 s cultures were perfused with alkaline imaging buffer (50 mM NH_4Cl substituted for 50 mM NaCl) to reveal total pHluorin fluorescence. Fluorescent images were captured at 4-s intervals throughout.

Plasma membrane-localized pHluorin reporters were revealed by bathing neurons in imaging buffer, and then perfusing with acidic imaging buffer (2-(N-morpholino)ethanesulfonic acid substituted for HEPES, pH 5.5) to quench surface fluorescence and retain background auto-fluorescence. Neurons were washed in imaging buffer and subsequently exposed to alkaline imaging buffer to reveal the total fluorescent signal. Where indicated, TTX (200 nM) was added to culture medium 72 h before imaging to block neuronal activity.

Imaging analysis
Offline data processing was performed using Fiji is just ImageJ (Fiji) software (Schindelin et al., 2012). For live-cell imaging, a script based on background thresholding was used to select nerve terminals, which placed regions of interest of identical size over those responding to stimulation. Average fluorescent intensity was measured over time using the time series analyzer plugin before screening regions of interest using a customized Java program that allows for visualization of the fluorescent responses and removal of aberrant traces from the data. Fixed cell images were analyzed by placing regions of interest of identical size over nerve terminals of transfected and untransfected cells and measuring the average fluorescent intensity in each channel. Transfected nerve terminals were normalized to measurements from surrounding untransfected neurons.

All subsequent data analyses were performed using Microsoft Excel, MATLAB, and GraphPad Prism 6.0 software. The change in activity-dependent pHluorin fluorescence was calculated as F/F_0 and normalized to the peak of stimulation. The percentage of pHluorin molecules visiting the plasma membrane during action potential stimulation was calculated

as F/F_0, and then expressed as a percentage of the pHluorin response in the presence of NH_4Cl. The fraction of pHluorin reporter at the plasma membrane was expressed as a percentage of total pHluorin and was calculated using the following equation: [(basal fluorescence – acidic fluorescence)/(alkaline fluorescence – acidic fluorescence)] × 100.

Super-resolution microscopy
Neurons transfected with either wild-type or R383Q SV2A-pHluorin were used 1–5 d post-transfection. Transfected neurons were imaged at 50 Hz and 20-ms exposure (16,000 frames) at 37°C on a Roper Scientific Ring-TIRF microscope with a CPI Apo 100×/1.49N.A. oil-immersion objective (Nikon Instruments). The microscope was equipped with Evolve 512 δ EMCCD cameras (Photometrics), a Perfect Focus System (Nikon Instruments), an iLas2 double laser illuminator (Roper Scientific), a quadruple beam splitter (ZT405/488/561/647rpc; Chroma Technology), and a QUAD emission filter (ZET405/488/561/640m; Chroma Technology).

Single particle tracking of surface molecules
Single plasma membrane SV2A molecules were imaged by performing Universal Point Accumulation Imaging in Nanoscale Topography (uPAINT; Giannone et al., 2010; Joensuu et al., 2017) on hippocampal neurons (DIV 15–20) in oblique illumination configuration. For uPAINT imaging, neurons were bathed in low KCl buffer (0.5 mM $MgCl_2$, 2.2 mM $CaCl_2$, 5.6 mM KCl, 145 mM NaCl, 5.6 mM D-glucose, 0.5 mM ascorbic acid, 0.1% BSA, and 15 mM HEPES; pH 7.4) and placed on the microscope. Following identification of transfected nerve terminals, low KCl buffer was replaced with stimulation buffer (substituted NaCl for KCl giving final concentrations of 56 mM KCl and 95 mM NaCl) containing 3.19 pg μl^{-1} anti-GFP Atto647N-tagged nanobodies (Synaptic Systems). Image acquisition was initiated during stimulation using a 642 nM laser to excite the nanobodies. Processing and analysis were conducted in PALMTracer 1, a custom written program that functions in MetaMorph (Molecular Devices; Kechkar et al., 2013; Nair et al., 2013). Regions of interest were drawn around nerve terminals of hippocampal axons based on pHluorin fluorescence unquenching during stimulation. The spatial detection limit was set to 0.106 μm. Mean square displacement (MSD) was calculated from reconstructed trajectories lasting a minimum of eight frames. The equation MSD(t) = a + 4Dt (where D = diffusion coefficient, a is y intercept, and t is time) was used to fit MSD. Trajectories were divided into mobile and immobile populations and a diffusion coefficient of $\log_{10} > -1.45$ μm^2 s^{-1} was considered as mobile (Constals et al., 2015; Joensuu et al., 2016).

Protein expression and GST-pull downs
Isolated nerve terminals (synaptosomes) from rat brain of either sex were prepared as described previously (Cousin and Robinson, 2000). GST fusion proteins were expressed in bacteria, lysed using sonication in the buffer (150 mM NaCl, 1 mM EDTA, 10% Triton X-100, 1.5% sarcosyl, 8 mg lysozyme, 1 mM PMSF, protease inhibitor cocktail, 5 mM dithiothreitol, and 10 mM Tris; pH 7.4) and then coupled to glutathione-sepharose beads (Anggono et al., 2006). Synaptosomes were solubilized for 5 min at 4°C in 25 mM Tris (pH 7.4), containing 1% Triton X-100, 150 mM NaCl, 1 mM EGTA, 1 mM EDTA, 1 mM PMSF, and protease inhibitor cocktail. Lysates were centrifuged at 20,442 × g for 5 min at 4°C with the supernatant retained. Supernatants were incubated with GST-fusion proteins for 1 h at 4°C to allow binding. After a series of washes in lysis buffer (including a wash in high-salt buffer, lysis buffer supplemented with 500 mM NaCl), beads were washed twice in 20 mM Tris (pH 7.4) and then boiled in SDS sample buffer. The released proteins separated by SDS-PAGE (12.5%) for subsequent analysis by Western blotting.

Co-immunoprecipitation from HEK cell cultures
HEK293 cells were maintained in culture media (MEM; Invitrogen, 41966-029), 10% FBS, and 1% penicillin/streptomycin at 37°C in 5% CO_2 humidified atmosphere. Cells were trypsinized (1× trypsin-EDTA, Invitrogen, 15400-054) and seeded into fresh 10-cm dishes 24 h before transfection with Lipofectamine 2000 as per manufacturer's instructions.
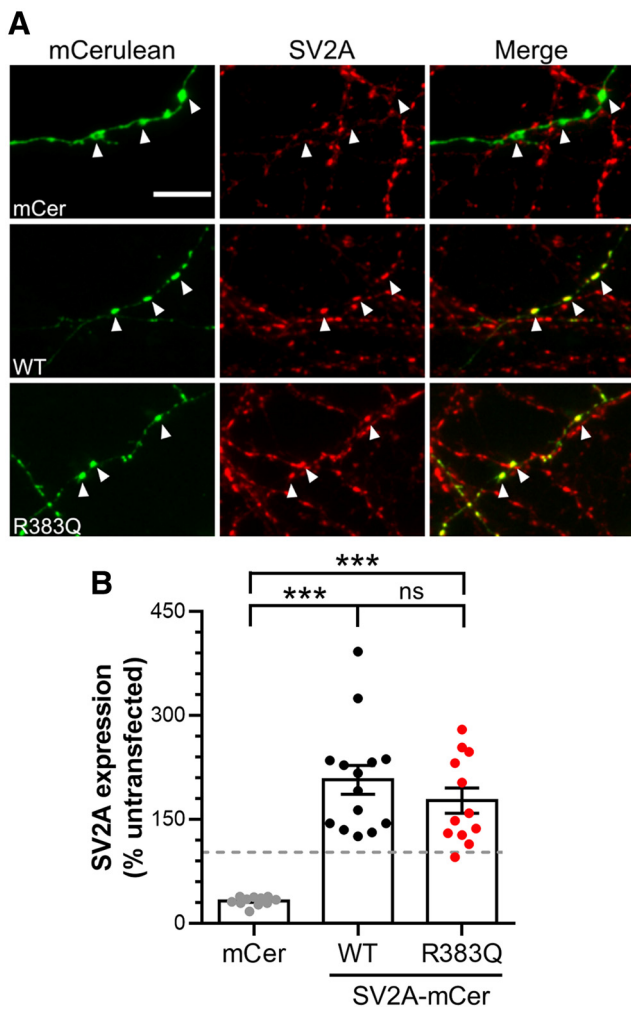
Figure 1. The R383Q mutation does not affect SV2A expression. Primary cultures of hippocampal neurons were transfected with shRNA against SV2A and either an empty vector (mCerulean, mCer), wild-type (WT) SV2A-mCer or R383Q SV2A-mCer after 7–9 DIV. After 13–15 DIV, neurons were fixed and immunostained for both GFP and SV2A. **A**, Example images are displayed, with GFP in green and SV2A in red. White arrowheads indicate transfected nerve terminals. Scale bar = 10 μm. **B**, Quantification of SV2A expression was performed by determining the intensity of SV2A signal in transfected synapses relative to untransfected synapses in the same field of view (n =12 mCer, n = 14 WT, n = 12 R383Q coverslips from three independent preparations, one-way ANOVA, ***$p < 0.001$, ns = not significant).

After transfection (48 h), cells were solubilized in 0.5 ml HEPES buffer for 1 h [50 mM HEPES (pH 7.5), 0.5% Triton X-100, 150 mM NaCl, 1 mM EDTA, 1 mM PMSF, and protease inhibitor cocktail) and centrifuged at 17,000 × g for 10 min to pellet the cell debris. Supernatant was collected then incubated with 10 μl of a 50% slurry of GFP TRAP beads (Chromotech) under rotation at 4°C for 2 h. Beads were washed three times with HEPES buffer before being incubated in SDS sample buffer at 65°C for 10 min to avoid SV2A protein aggregation. Samples were then analyzed by SDS-PAGE and Western blotting.

Western blotting
Western blotting was performed as described previously (Anggono et al., 2006). Primary antibodies used were anti-GFP rabbit (ab6556, 1:4000) and anti-HA rabbit (ICLlab, RHGT-45A-Z, 1:20,000) or rabbit anti-Syt1 (Synaptic Systems, #105103, 1:5000). IRDye secondary antibodies [800CW anti-rabbit IgG (#925-32213, 1:10,000); 680RD anti-rabbit IgG (#926-68071, 1:10,000), and Odyssey blocking PBS buffer (#92740000)] were from LI-COR Biosciences. Blots were visualized using a LiCOR Odyssey fluorescent imaging system (LiCOR Biotechnology). Band densities were determined using
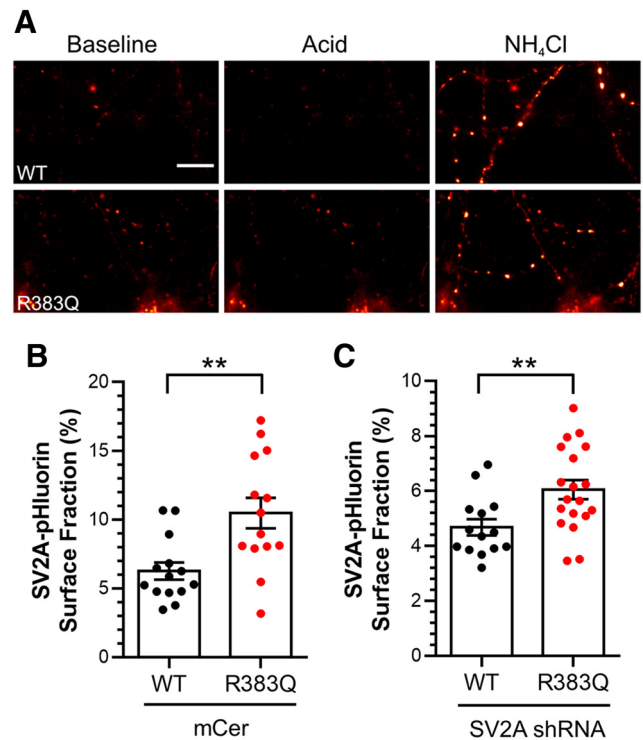

Figure 2. SV2A R383Q is mislocalized from SVs. Primary cultures of hippocampal neurons were transfected with either wild-type or R383Q SV2A-pHluorin and either empty mCer vector or shRNA against SV2A 7–8 d before image acquisition (DIV 13–15). Cultures were sequentially perfused with acidic then NH₄Cl imaging buffer, interspersed with control imaging buffer. **A**, Example images are displayed from neurons expressing both SV2A shRNA and SV2A-pHluorin with pseudo-coloring to indicate regions of high fluorescent intensity in control (Baseline), acidic (Acid), and NH₄Cl imaging buffer. Scale bar = 10 μm. **B**, **C**, The proportion of SV2A-pHluorin on the plasma membrane as a percentage of the total pool is presented ±SEM in the presence (**B**) or absence (**C**) of endogenous SV2A [**B**; n = 14 wild-type (WT) and R383Q, **C**; n = 15 WT, n =19 R383Q, cells from three independent preparations, Student's t test, **p = 0.003 for **B**, **p = 0.008 for **C**].

LiCOR Image Studio Lite software (version 5.2). GST pulldown samples were analyzed by normalizing the density of the Western blotting bands to the density of GST fusion protein band revealed by Ponceau-S staining. For co-immunoprecipitations, the amount Syt1-HA co-immunoprecipitated was normalized to the amount of input protein. These values were then normalized to the amount of immunoprecipitated SV2A-mCerulean.

Statistical analysis
Statistical analysis was performed in Graph Pad Prism 6.0. A Student's t test was used to compare differences between two groups, whereas a one-way ANOVA with a Tukey's *post hoc* test was used to compare more than two groups. In all analyses, the sample size (n) was taken to be the number of independent experiments or individual coverslips. All data are presented as mean values ± SEM.

Results

The R383Q mutation does not affect SV2A expression at nerve terminals

Loss of SV2A in mice results in seizure activity and early lethality (Crowder et al., 1999; Janz et al., 1999). It also disrupts the trafficking and expression of Syt1 (Yao et al., 2010; Kaempf et al., 2015; Zhang et al., 2015). Whether these two outcomes of SV2A dysfunction are linked is still unknown. The identification of a patient with intractable epilepsy possessing a homozygous mutation (R383Q) in SV2A (Serajee and Huq, 2015) provides the opportunity to address this question directly.

We first determined whether the R383Q mutation resulted in altered expression of SV2A at nerve terminals in primary cultures of hippocampal neurons. To determine this, endogenous SV2A was depleted using shRNA and co-expressed with either shRNA-resistant wild-type or R383Q SV2A tagged with the fluorescent protein mCerulean (mCer; Fig. 1A). Expression of shRNA against SV2A resulted in a significant depletion of SV2A at nerve terminals when compared with untransfected controls (Fig. 1B; one-way ANOVA, $p < 0.0001$), as observed previously (Zhang et al., 2015). Co-expression of wild-type SV2A-mCer restored expression to approximately two-fold that of endogenous levels (Fig. 1B; one-way ANOVA, $p < 0.0001$). Similar values were also observed for R383Q SV2A-mCer, indicating that this mutation does not alter SV2A expression at nerve terminals (Fig. 1B; one-way ANOVA, not significant).

The R383Q mutation increases SV2A plasma membrane stranding

We next determined whether the R383Q mutation affected the localization of SV2A at nerve terminals. To do so, we exploited SV2A-pHluorin, a genetically-encoded reporter that provides information on the pH of its local environment due to a pH-sensitive GFP fused to a lumenal loop of SV2A (Zhang et al., 2015). In resting neurons, SV2A-pHluorin is only fluorescent when present at the plasma membrane, since its fluorescence is quenched within the acidic SV interior. Therefore, exposure to an impermeant acidic solution can reveal the proportion of SV2A on the plasma membrane. The extent of surface SV2A-pHluorin can then be expressed as a proportion of the total pool by de-acidifying SVs with an ammonium chloride solution (Fig. 2A; Gordon et al., 2011; Zhang et al., 2015).

When expressed in wild-type neurons, the plasma membrane localization of SV2A-pHluorin was low ($6.3 \pm 0.6\%$ of total; Fig. 2B), in agreement with previous studies (Pan et al., 2015). In contrast, R383Q SV2A-pHluorin displayed an approximate two-fold increase ($10.5 \pm 1.2\%$ of total; Fig. 2B, Student's t test, $p = 0.003$). When either wild-type or R383Q SV2A-pHluorin were expressed in neurons which had endogenous SV2A depleted using shRNA (to mimic the homozygous condition), the proportion of surface R383Q SV2A-pHluorin was still significantly increased (Fig. 2C, Student's t test, $p = 0.008$). Therefore, the R383Q mutation results in mislocalization of SV2A from SVs to the plasma membrane in neurons that were either depleted of, or contained, endogenous SV2A.

To gain additional insight into the increased surface stranding of R383Q SV2A, we determined whether this mutation resulted
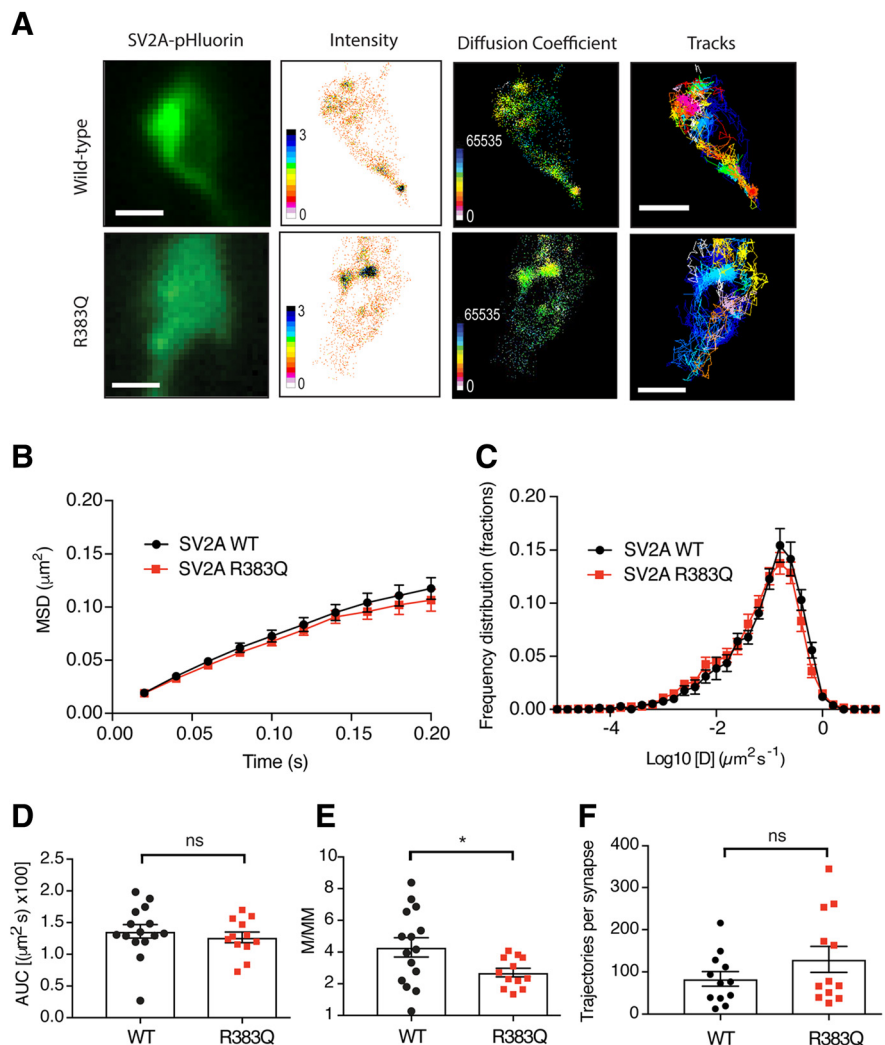

Figure 3. The R383Q mutation impacts the plasma membrane mobility of SV2A at nerve terminals. Primary cultures of hippocampal neurons were transfected with either wild-type or R383Q SV2A-pHluorin at 14–15 DIV. After 1–5 d post-transfection, neurons were stimulated 50 mM KCl. **A**, Representative panels depicting presynaptic SV2A-pHluorin fluorescence in addition to diffusion coefficient, intensity, and tracks of SV2A-pHluorin wild-type (WT; $n = 15$) and R383Q ($n = 12$; >3 independent preparations). Scale bar = 1 μm. **B**, MSD of SV2A-pHluorin-atto647N-nanobodies (NB). **C**, Frequency distribution of $\log_{10}$ of diffusion coefficient [D] (μm^2 s^{-1}). **D**, Area under the curve (AUC; μm^2 × 100) for MSD of SV2A-pHluorin (WT/R383Q) shown in **B**. **E**, Mobile:immobile ratio (M/MM) for frequency distribution shown in **C**. **F**, Number of trajectories of wild-type and R383Q SV2A-pHluorin ($n = 12$ neurons) per synapse. Values are represented as mean ± SEM. Statistical comparisons were performed using a paired Student's t test. No significant differences detected between AUC of MSD (**D**; ns, $p = 0.50$) and detections per synapse (**F**; *$p = 0.20$) for SV2A-pHluorin WT and R383Q. Significant difference observed between WT and R383Q mutant for the mobile:immobile ratio (**E**; ns, $p = 0.037$).

in altered SV2A mobility at the plasma membrane using the single molecule super-resolution microscopy technique, uPAINT (Giannone et al., 2010; Joensuu et al., 2017). Neurons transfected with either wild-type or R383Q SV2A-pHluorin were imaged during stimulation in the presence of anti-GFP Atto647N nanobodies (Fig. 3A). Single-particle tracking analysis was performed to generate high-resolution mean intensities, diffusion coefficients, and single-molecule trajectory maps of either wild-type or R383Q SV2A–pHluorin (Fig. 3B–F). No significant differences in the MSD (Fig. 3D, Student's t test, $p = 0.5$) and number of detected trajectories per synapse of R383Q SV2A-pHluorin-atto647-NB mobility (Fig. 3F, Student's t test, $p = 0.2$) was observed compared with wild type. However, a difference in the mobile:immobile ratio was detected, with the R383Q SV2A-pHluorin displaying a lower mobility than wild type (Fig. 3E,
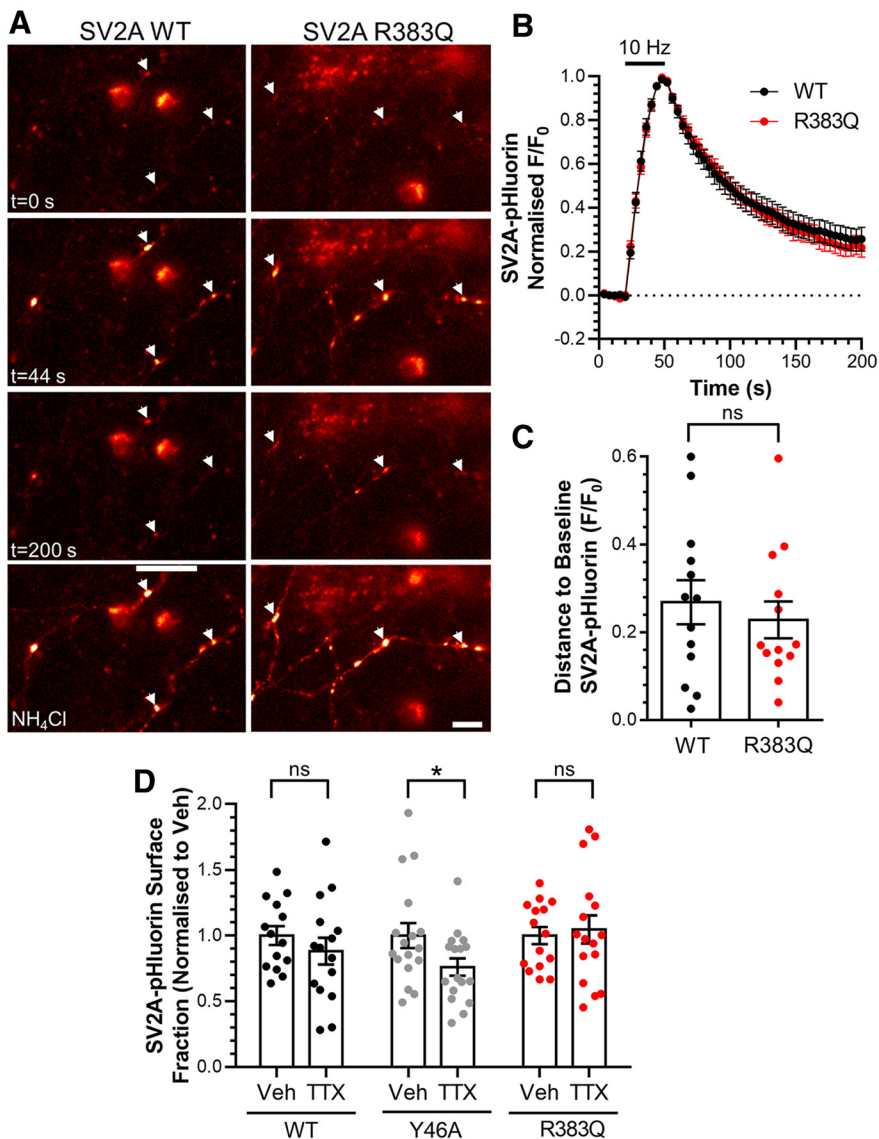
Figure 4. Mislocalization of R383Q SV2A is not due to an activity-dependent trafficking defect. *A–C*, Primary cultures of hippocampal neurons were transfected with both SV2A-pHluorin (wild-type or R383Q) and shRNA against SV2A after 7–8 DIV. After 13–15 DIV neurons were stimulated with a train of 300 action potentials delivered at 10 Hz. The neurons were allowed to recover before being pulsed with NH_4Cl imaging buffer to reveal the total SV2A-pHluorin population. *A*, Representative images are displayed in at specific time points indicated, with responsive nerve terminals highlighted using arrowheads. Scale bar = 10 μm. *B*, Traces display the time course of the average fluorescent SV2A-pHluorin response normalized to the peak of stimulation. Bar indicates the period of stimulation. *C*, SV2A-pHluorin remaining to be retrieved 130 s after termination of stimulation is displayed as F/F_0 ±SEM (for *B*, *C*, $n = 13$ neurons from three independent preparations, displayed ±SEM, Student's t test, ns, $p = 0.917$). *D*, Primary cultures of hippocampal neurons were transfected with mCerulean and either wild-type, Y46A, or R383Q SV2A-pHluorin at 7 DIV. Neurons were treated with either vehicle (Veh) or TTX (200 nM) at 11 DIV for 72 h. Cultures then sequentially perfused with acidic and NH_4Cl imaging buffer, interspersed with control imaging buffer. The proportion of SV2A-pHluorin on the plasma membrane expressed as a percentage of the total pool normalized to the control condition ±SEM is displayed ($n = 14$–17 cells from four independent preparations, Student's t test, ns, $p = 0.375$ WT, *$p = 0.046$ Y46A, ns, $p = 0.716$ R383Q).

Student's t test, $p = 0.038$). In the diffusion coefficient maps (Fig. 3A), regions highlighted in warmer colors are associated with tracks of low mobility, which were more prominent for SV2A-R383Q-pHluorin relative to SV2A-WT-pHluorin. Taken together, this suggests that the R383Q mutation reduces SV2A mobility on the plasma membrane, potentially via increased clustering.

Increased plasma membrane localization of SV proteins can be indicative of defective retrieval during endocytosis.

Therefore, we next determined whether the R383Q mutation disrupted SV2A retrieval during endocytosis in SV2A-depleted neurons. The activity-dependent trafficking of SV2A-pHluorin can be detected as an increase in fluorescence on stimulation due to exocytosis (since the reporter encounters the neutral extracellular environment; Fig. 4A). After stimulation terminates, the kinetics of the fluorescence decay reflects the kinetics of SV2A-pHluorin retrieval, since endocytosis is rate limiting when compared with SV acidification (Atluri and Ryan, 2006; Granseth et al., 2006; but also see Egashira et al., 2015). When neurons expressing wild-type SV2A-pHluorin were challenged with a train of action potentials (300 at 10 Hz), a characteristic peak and fluorescent decay was observed (Fig. 4B). An identical response was observed for R383Q SV2A-pHluorin (Fig. 4B). An absence of effect of the R383Q mutation on SV2A retrieval was confirmed when the proportion of pHluorin reporter remaining on the plasma membrane after stimulation was quantified (Fig. 4C, Student's t test, $p = 0.917$). Furthermore, the R383Q mutation had no effect on the number of SV2A-pHluorin molecules visiting the plasma membrane during stimulation (wild type, 53.1 ± 3.4%; 53.6 ± 3.9% of total SV2A-pHluorin, Student's t test, $p = 0.91$), indicating an absence of effect on SV exocytosis. Thus, the R383Q mutation results in a mislocalization of SV2A from SVs to the plasma membrane, but had no effect on its retrieval during endocytosis. Importantly, this also indicates that the R383Q mutation does not affect endocytosis in general, since any disruption would be reflected in altered SV2A-pHluorin retrieval kinetics.

To confirm that the increased proportion of the R383Q mutant residing at the plasma membrane was not due to defects in its activity-dependent retrieval, we examined the effect of silencing neuronal activity. This maneuver typically corrects surface stranding defects that are a result of activity-dependent cargo retrieval (Kaempf et al., 2015). Neuronal activity was silenced via application of the sodium channel antagonist TTX for 72 h. Neuronal silencing had no effect on the proportion of wild-type SV2A-pHluorin at the plasma membrane (Fig. 4D, Student's t test, $p = 0.375$). In contrast, an internalization defective SV2A mutant (Y46A; Yao et al., 2010) displayed a reduced plasma membrane localization in TTX-treated cultures when compared with control (Fig. 4D, Student's t test, $p = 0.046$). Finally, silencing of neuronal activity had no effect on the mislocalization of R383Q SV2A-pHluorin (Fig. 4D,

Student's t test, $p = 0.716$). This confirmed that the increased plasma membrane localization of the R383Q mutant was not due to defective activity-dependent retrieval.

The R383Q mutation disrupts SV2A binding to Syt1

SV2A interacts with the C2B domain of Syt1 via its N terminus in a phosphorylation-dependent manner (Schivell et al., 1996, 2005; Pyle et al., 2000; Zhang et al., 2015). This interaction controls a series of Syt1-specific functions in neurons (Ciruelas et al., 2019). The R383Q mutation resides on a large cytoplasmic loop that is distal from the SV2A N terminus in terms of its primary sequence (Fig. 5A). However, due to the key role SV2A performs in the control of Syt1 function, we assessed the impact of the R383Q mutation on this interaction.

First, we determined whether the cytoplasmic loop of SV2A in which the R383Q mutation resides interacts with Syt1. To achieve this, we generated a GST-fusion protein encompassing this loop (residues 356–447; Fig. 5A) with which we attempted to extract Syt1 from nerve terminal lysates. Pull-down experiments were performed using either GST alone, wild-type GST-SV2A$_{356-447}$ or the equivalent R383Q mutant. Western blotting revealed that neither wild-type nor the R383Q mutant was able to extract Syt1 from nerve terminal lysates that had either been challenged with or without elevated KCl (Fig. 5B). Therefore, the third cytoplasmic loop of SV2A is not sufficient to bind Syt1.

We next examined whether the R383Q mutation affected the ability of full-length SV2A to interact with Syt1 in a heterologous expression system. Both SV2A-mCer and HA-tagged Syt1 were co-expressed in HEK cells with SV2A-mCer subsequently immunoprecipitated using an anti-GFP nanobody. Wild-type SV2A-mCer co-immunoprecipitated HA-Syt1, whereas no HA-Syt1 was present in immunoprecipitates from cells expressing mCer alone (Fig. 5C,D). R383Q SV2A-mCer was able to co-immunoprecipitate HA-Syt1, however, at a significantly reduced level (Fig. 5D, Student's t test, $p = 0.0035$). Therefore, the R383Q mutation results in a decreased ability of SV2A to interact with Syt1.

The R383Q mutation disrupts the expression and activity-dependent trafficking of Syt1

The reduced interaction of Syt1 with the R383Q mutant form of SV2A suggests that it may alter Syt1 function in the absence of endogenous SV2A. We first determined whether R383Q SV2A-mCer affected the synaptic expression of Syt1 in SV2A-depleted neurons (Fig. 6A). Knock-down of SV2A reduced endogenous Syt1 levels below that of untransfected controls, using synaptophysin as a presynaptic marker (Fig. 6B; Yao et al., 2010; Kaempf et al., 2015). Conversely, rescue of expression with wild-type SV2A-mCer produced a significant increase in endogenous Syt1 expression when compared with SV2A-depleted neurons (Fig. 6B, one-way ANOVA, $p = 0.0002$). In contrast, expression of R383Q SV2A-mCer was unable to restore endogenous Syt1 expression to these levels (Fig. 6B, one-way ANOVA, $p = 0.007$). Therefore, the
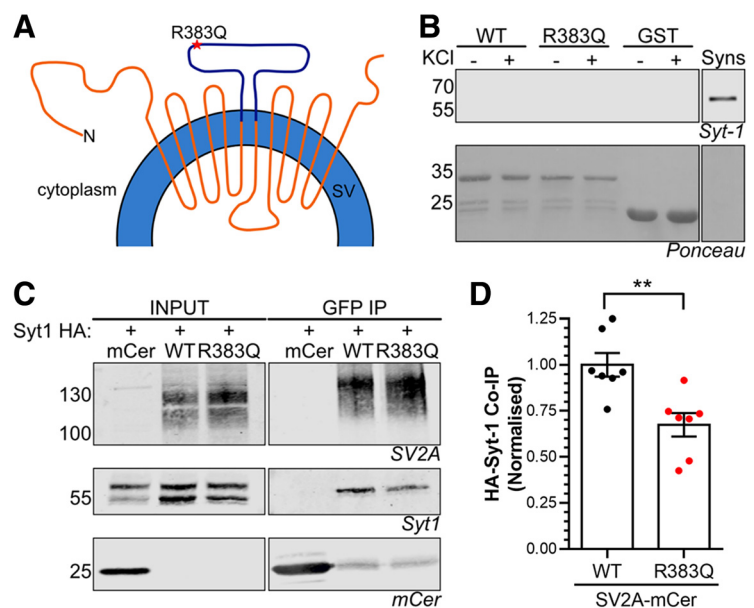

Figure 5. SV2A R383Q displays reduced binding to Syt1. **A**, Diagram depicts SV2A in the SV membrane with the cytoplasmic loop fused to GST highlighted in purple. **B**, Glutathione beads coupled to either GST alone, wild-type (WT) GST-SV2A$_{356-447}$ or R383Q GST-SV2A$_{356-447}$ were used to extract interaction partners from nerve terminal lysates which had previously been challenged with or without 30 mM KCl. A representative western blot is displayed for Syt1 in addition to Ponceau staining to reveal GST fusion proteins. Synaptosome lysates (Syns) were also present as a positive control (representative of five independent experiments). **C, D**, HA-tagged Syt1 was co-expressed with either mCerulean empty vector (mCer), WT SV2A-mCer or R383Q SV2A-mCer in HEK cells. Immunoprecipitation of mCer was performed from cell lysates. **C**, Representative western blots displaying the amount of SV2A, Syt1, or mCer present in either the input (2.5%) or immunoprecipitate. **D**, Quantification of the amount of HA-Syt1 co-immunoprecipitated (co-IP) was normalized to the amount of SV2A-mCer ± SEM ($n = 7$, Student's t test, **$p = 0.0035$).

R383Q mutant has lost the ability to regulate Syt1 expression at nerve terminals.

Loss of SV2A results in an acceleration of activity-dependent Syt1-pHluorin retrieval during endocytosis (Kaempf et al., 2015; Zhang et al., 2015). Therefore, we next determined whether the R383Q mutation could rescue Syt1 retrieval kinetics in SV2A-depleted neurons (Fig. 7A). Depletion of SV2A with shRNA resulted in an acceleration of Syt1-pHluorin retrieval, a phenotype that was rescued by wild-type SV2A-mCer (Fig. 7B,C, one-way ANOVA, $p = 0.0348$). In contrast, expression of R383Q SV2A-mCer was unable to rescue normal Syt1-pHluorin retrieval kinetics (Fig. 7B,C, one-way ANOVA, $p = 0.0473$). Therefore, the R383Q mutation results in a version of SV2A that has lost the ability to control the retrieval of Syt1 during neuronal activity.

Discussion

Loss of SV2A function is linked to epilepsy, since mice that are null for the gene exhibit lethal seizure activity (Crowder et al., 1999; Janz et al., 1999). However, it is still unclear how loss of SV2A function translates into seizures. To investigate this, we examined the effect of expressing a human SV2A mutant linked to epilepsy in primary neuronal cultures that were depleted of endogenous SV2A to determine which presynaptic events were altered. We found that the R383Q mutation caused mislocalization of SV2A from SVs to the plasma membrane in a manner independent of neuronal activity. The mutation reduced the ability of SV2A to bind to Syt1, and failed to correct defects in the expression and activity-dependent trafficking of Syt1. This links inaccurate control of Syt1 function by SV2A with seizure generation and epilepsy.
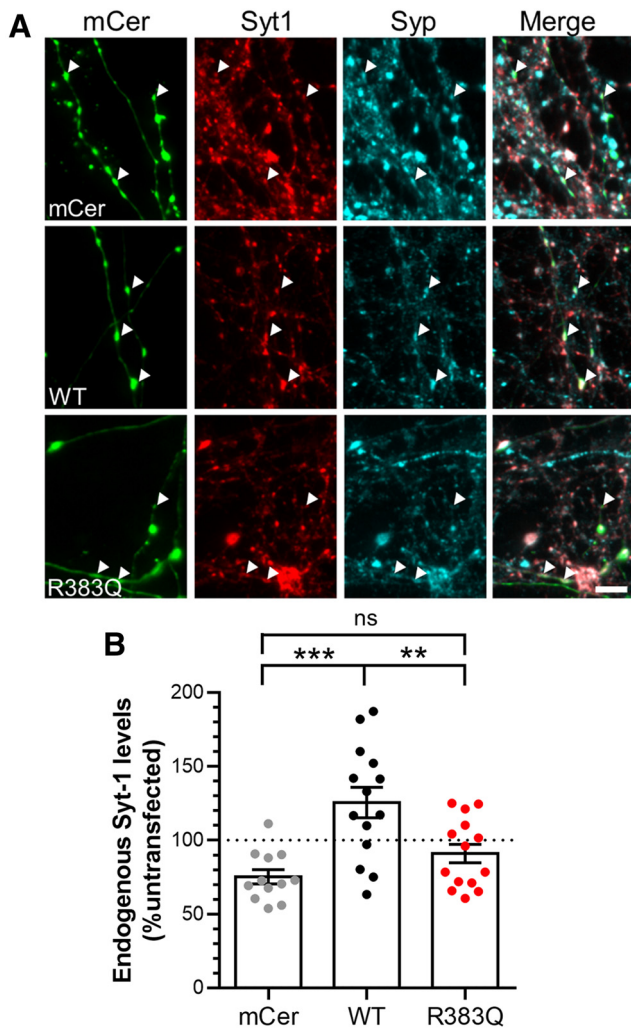
Figure 6. SV2A R383Q cannot rescue Syt1 expression in SV2A-depleted cells. Cultured hippocampal neurons were transfected with SV2A shRNA and either an empty vector (mCerulean, mCer), wild-type (WT) SV2A-mCer, or R383Q SV2A-mCer at 7–9 DIV. After 13–15 DIV, neurons were fixed and immunostained for GFP, Syt1, and Synaptophysin (Syp). **A**, Representative images are displayed with arrowheads highlighting transfected nerve terminals (identified using Syp immunostaining). Scale bar = 10 μm. **B**, Quantification of Syt1 expression at nerve terminals is displayed, with the signal from transfected synapses normalized to untransfected synapses in the same field of view ± SEM ($n = 12$ mCer, $n = 14$ WT, $n = 14$ R383Q cells from three independent preparations, one-way ANOVA, ***$p = 0.0002$, **$p = 0.007$, ns = not significant).

SV2A is one of the most efficiently targeted proteins to SVs, with only ~5% present at the plasma membrane in resting neurons (Pan et al., 2015). This is similar to the vesicular glutamate transporter, whereas other cargoes such as synaptophysin, synaptobrevin-II and Syt1 have a higher baseline level of surface localization (Gordon et al., 2011; Kononenko et al., 2013; Kaempf et al., 2015; Pan et al., 2015; Zhang et al., 2015; Harper et al., 2017). The activity-independent increase in surface stranding of the R383Q mutant is intriguing, suggesting that mislocalization results from either an increased retention at the plasma membrane or loss from SVs via an unidentified mechanism. The decrease in the ratio of mobile:immobile SV2A R383Q molecules suggests the former possibility. SV2A molecules stranded on the plasma membrane have a similar mobility to synaptobrevin-II (Joensuu et al., 2016, 2017), suggesting that the organization of these vesicular proteins at the nanoscale level might be dynamically regulated. Both the increased retention of R383Q SV2A and
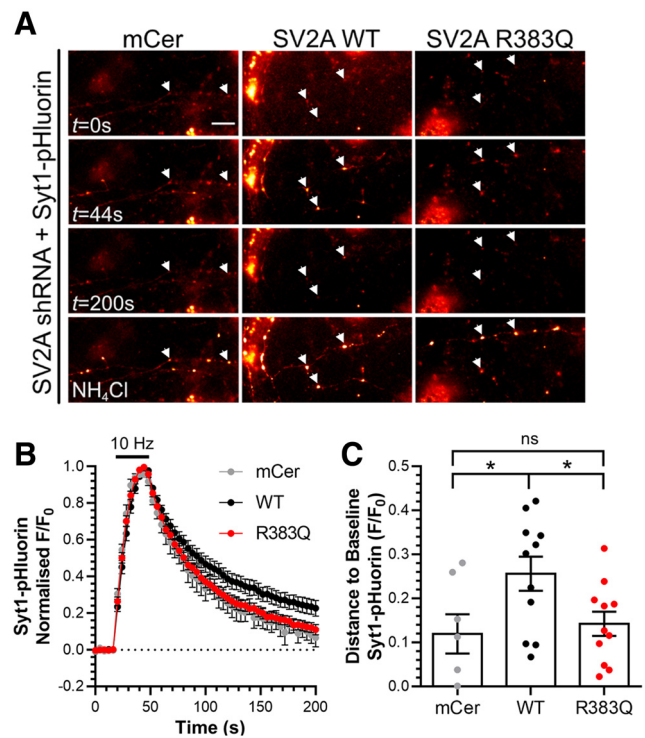

Figure 7. SV2A R383Q cannot rescue Syt1 retrieval kinetics in SV2A-depleted cells. Primary cultures of hippocampal neurons were transfected with a bicistronic vector expressing Syt1-pHluorin (Syt1-pH) and shRNA against SV2A and either mCerulean (mCer), wild-type (WT) SV2A-mCer, or R383Q SV2A-mCer after 7–8 DIV. At 13–15 DIV, neurons were stimulated with a train of 300 action potentials delivered at 10 Hz. Neurons were allowed to recover before being pulsed with NH$_4$Cl imaging buffer reveal the total Syt1-pH population. **A**, Representative images are displayed at specific time points indicated, with responsive nerve terminals highlighted using arrowheads. Scale bar = 10 μm. **B**, Traces display the time course of the average fluorescent Syt1-pHluorin response normalized to the peak of stimulation. Bar indicates the period of stimulation ($n = 7$ for mCer and $n = 11$ for both WT and R383Q SV2A-mCer, from four independent preparations). **C**, Syt1-pHluorin remaining to be retrieved 130 s after termination of stimulation is displayed as F/F$_0$ ±SEM (one-way ANOVA, *$p = 0.0348$ WT compared with mCer, $p = 0.0473$ WT compared with R383Q SV2A-mCer, ns = not significant, mCer compared with R383Q).

altered nanoclustering may occur via enhanced interactions with integral plasma membrane proteins or the presynaptic cytoskeletal network. These cell surface phenotypes may not be critical to the epilepsy presented in this individual however, since the mutant appears to behave in a loss of function manner.

To replicate the homozygous human condition in which the R383Q mutation was identified (Serajee and Huq, 2015) experiments were performed in neurons where endogenous SV2A was depleted. In this regard, knock-down of endogenous SV2A expression was very efficient (Zhang et al., 2015) and rescue of expression by either shRNA-resistant wild-type or R383Q SV2A-mCer did not exceed a two-fold increase over endogenous levels, ensuring a close approximation to the disease context. Coincidentally, a new heterozygous missense mutation in the *SV2A* gene has recently been identified in a child and mother with epilepsy (Wang et al., 2019). The mutation (R570C) is located within the large intraluminal loop of SV2A, a region that when mutated can result in defective SV2A trafficking (Ciruelas et al., 2019). This heterozygous mutation is likely to be dominant, since only the homozygous R383Q mutation results in loss of function (Serajee and Huq, 2015), however it should be noted that haploinsufficient SV2A mice display increased lethality compared with wild type (Crowder et al., 1999; Janz et al., 1999).

SV2A binds adenine nucleotides within its third cytoplasmic loop, with the R383Q mutation residing at the extreme periphery of one of the potential interaction motifs (Yao and Bajjalieh, 2008). This binding is not related to ATP transport per se, and has been proposed to alter the ability of SV2A to interact with other proteins (Ciruelas et al., 2019). Regardless, altered adenine nucleotide binding is unlikely to be responsible for our observed effects, since binding is still retained when the region containing R383 is deleted (Yao and Bajjalieh, 2008). The R383Q mutation does result in a decreased interaction between SV2A and Syt1, however the cytoplasmic loop containing the mutation is not sufficient to bind Syt1. Therefore, this loop may modulate binding via the SV2A N terminus, which contains Syt1 interaction sites (Schivell et al., 1996, 2005; Zhang et al., 2015).

The R383Q mutation had no effect on the activity-dependent trafficking of SV2A. Furthermore, it had no global effect on SV exocytosis or endocytosis. The absence of effect on SV endocytosis has been observed by different groups (Yao et al., 2010; Kaempf et al., 2015; Zhang et al., 2015), suggesting the major role of SV2A is to coordinate Syt1 expression and trafficking. The ability of SV2A to interact with Syt1 appears to be central in the control of its function, since the R383Q mutant displayed a marked inability to rescue either Syt1 expression or activity-dependent Syt1 retrieval. This is also true for the T84A SV2A mutant (C.H., unpublished observations), which cannot interact with Syt1 (Zhang et al., 2015). Therefore, we propose that the primary defect of the R383Q mutation is the reduction in Syt1 binding, which results in decreased Syt1 expression and trafficking. The failure of the R383Q mutant to rescue these functions suggests that these may be interlinked, e.g., lower levels of Syt1 may result in its more efficient retrieval. If this is the case, then the primary dysfunction caused by the decreased interaction of SV2A with Syt1 is the control of Syt1 expression. Testing whether Syt1 retrieval kinetics are affected by reducing its expression is complex however, since monitoring trafficking using Syt1-pHluorin will also increase Syt1 levels.

The patient carrying the homozygous R383Q mutation displayed early developmental delay, including microcephaly, growth retardation and severe hypotonia within six months (Serajee and Huq, 2015). Seizures were reported at two months, and were subsequently refractory to medication. Recently, a Syt1-specific disorder has been identified, named Baker–Gordon syndrome (Baker et al., 2018). Patients with Baker–Gordon syndrome display hypotonia, hyperkinetic movement disorders, and developmental delay, which range from moderate to profound. All patients have heterozygous missense mutations in the calcium-binding C2B domain of Syt1, resulting in reduced SV fusion kinetics (Baker et al., 2015, 2018). Importantly, no patient displayed epileptic seizures. The absence of seizures in Baker–Gordon patients suggests that Syt1 dysfunction is not sufficient for epilepsy, but rather the decrease in the trafficking or expression of Syt1 in the absence of functional SV2A may be key. It will be critical for future studies to investigate the interplay between these two important SV proteins in both the physiological and pathologic context.

A link between SV2A dysfunction and seizure activity is well established. For example, postmortem samples from patients with temporal lobe epilepsy displayed reduced SV2A expression in the hippocampus, a finding mirrored in rodent models of status epilepticus (van Vliet et al., 2009). Furthermore, SV2A knock-out mice display lethal seizure activity after three weeks (Crowder et al., 1999; Janz et al., 1999) and rats expressing a spontaneous missense mutation in SV2A display increased

seizure susceptibility (Tokudome et al., 2016a,b). Importantly, both of these model systems displayed a reduction in Syt1 expression across the whole brain of ~50% (Yao et al., 2010; Tokudome et al., 2016b). Furthermore, SVs purified from SV2A/B double knock-out mice displayed an 85% reduction in Syt1 (Yao et al., 2010). Therefore, there is a good correlation between the reduction in Syt1 expression and seizure activity in rodents with dysfunctional or absent SV2A.

How may seizure activity originate? One potential mechanism is from the combination of reduced Syt1 expression and its further reduction on SVs. This depletion may only affect neurons that fire at high frequencies, such as inhibitory interneurons, (Bartos et al., 2007), due to an increased demand for efficient Syt1 trafficking from an already reduced pool of Syt1 molecules. Importantly, SV2A is the primary paralog in GABAergic neurons (Ciruelas et al., 2019) and expression of SV2A is higher in GABAergic neurons when compared with glutamatergic neurons (Tokudome et al., 2016a,b). In addition, rats expressing a spontaneous missense mutation in SV2A display a defect in the evoked release of GABA, but not glutamate (Tokudome et al., 2016a,b). Therefore, since GABAergic interneurons fire at higher frequencies they may experience an exacerbated depletion of Syt1 from SVs, whereas most neurons may be able to function normally. The loss of Syt1 from GABAergic SVs may result in a reduction in the rate, extent or synchronicity of SV fusion events. This may culminate in a loss of inhibitory drive in specific circuits, resulting in seizure activity.

In conclusion, we have demonstrated that a missense mutation in SV2A that results in human epilepsy is unable to rescue defects in Syt1 function when expressed in its disease-related context. This strongly suggests that dysregulation of Syt1 function may be responsible for the seizure activity observed due to loss of SV2A function.

References

Anggono V, Smillie KJ, Graham ME, Valova VA, Cousin MA, Robinson PJ (2006) Syndapin I is the phosphorylation-regulated dynamin I partner in synaptic vesicle endocytosis. Nat Neurosci 9:752–760.

Atluri PP, Ryan TA (2006) The kinetics of synaptic vesicle reacidification at hippocampal nerve terminals. J Neurosci 26:2313–2320.

Baker K, Gordon SL, Grozeva D, van Kogelenberg M, Roberts NY, Pike M, Blair E, Hurles ME, Chong WK, Baldeweg T, Kurian MA, Boyd SG, Cousin MA, Raymond FL (2015) Identification of a human synaptotagmin-1 mutation that perturbs synaptic vesicle cycling. J Clin Invest 125:1670–1678.

Baker K, Gordon SL, Melland H, Bumbak F, Scott DJ, Jiang TJ, Owen D, Turner BJ, Boyd SG, Rossi M, Al-Raqad M, Elpeleg O, Peck D, Mancini GMS, Wilke M, Zollino M, Marangi G, Weigand H, Borggraefe I, Haack T, et al. (2018) SYT1-associated neurodevelopmental disorder: a case series. Brain 141:2576–2591.

Bartos M, Vida I, Jonas P (2007) Synaptic mechanisms of synchronized gamma oscillations in inhibitory interneuron networks. Nat Rev Neurosci 8:45–56.

Chanaday NL, Cousin MA, Milosevic I, Watanabe S, Morgan JR (2019) The synaptic vesicle cycle revisited: new Insights into the modes and mechanisms. J Neurosci 39:8209–8216.

Ciruelas K, Marcotulli D, Bajjalieh SM (2019) Synaptic vesicle protein 2: a multi-faceted regulator of secretion. Semin Cell Dev Biol 95:130–141.

Constals A, Penn AC, Compans B, Toulmé E, Phillipat A, Marais S, Retailleau N, Hafner AS, Coussen F, Hosy E, Choquet D (2015) Glutamate-induced AMPA receptor desensitization increases their mobility and modulates short-term plasticity through unbinding from Stargazin. Neuron 85:787–803.

Cousin MA, Robinson PJ (2000) Ca(2+) influx inhibits dynamin and arrests synaptic vesicle endocytosis at the active zone. J Neurosci 20:949–957.

Crowder KM, Gunther JM, Jones TA, Hale BD, Zhang HZ, Peterson MR, Scheller RH, Chavkin C, Bajjalieh SM (1999) Abnormal

neurotransmission in mice lacking synaptic vesicle protein 2A (SV2A). Proc Natl Acad Sci USA 96:15268–15273.

Egashira Y, Takase M, Takamori S (2015) Monitoring of vacuolar-type H+ ATPase-mediated proton influx into synaptic vesicles. J Neurosci 35:3701–3710.

Geppert M, Goda Y, Hammer RE, Li C, Rosahl TW, Stevens CF, Südhof TC (1994) Synaptotagmin I: a major Ca2+ sensor for transmitter release at a central synapse. Cell 79:717–727.

Giannone G, Hosy E, Levet F, Constals A, Schulze K, Sobolevsky AI, Rosconi MP, Gouaux E, Tampé R, Choquet D, Cognet L (2010) Dynamic superresolution imaging of endogenous proteins on living cells at ultra-high density. Biophys J 99:1303–1310.

Gordon SL, Cousin MA (2013) X-linked intellectual disability-associated mutations in synaptophysin disrupt synaptobrevin II retrieval. J Neurosci 33:13695–13700.

Gordon SL, Cousin MA (2016) The iTRAPs: guardians of synaptic vesicle cargo retrieval during endocytosis. Front Synaptic Neurosci 8:1.

Gordon SL, Leube RE, Cousin MA (2011) Synaptophysin is required for synaptobrevin retrieval during synaptic vesicle endocytosis. J Neurosci 31:14032–14036.

Granseth B, Odermatt B, Royle SJ, Lagnado L (2006) Clathrin-mediated endocytosis is the dominant mechanism of vesicle retrieval at hippocampal synapses. Neuron 51:773–786.

Harper CB, Mancini GMS, van Slegtenhorst M, Cousin MA (2017) Altered synaptobrevin-II trafficking in neurons expressing a synaptophysin mutation associated with a severe neurodevelopmental disorder. Neurobiol Dis 108:298–306.

Janz R, Goda Y, Geppert M, Missler M, Südhof TC (1999) SV2A and SV2B function as redundant Ca2+ regulators in neurotransmitter release. Neuron 24:1003–1016.

Joensuu M, Padmanabhan P, Durisic N, Bademosi AT, Cooper-Williams E, Morrow IC, Harper CB, Jung W, Parton RG, Goodhill GJ, Papadopulos A, Meunier FA (2016) Subdiffractional tracking of internalized molecules reveals heterogeneous motion states of synaptic vesicles. J Cell Biol 215:277–292.

Joensuu M, Martínez-Mármol R, Padmanabhan P, Glass NR, Durisic N, Pelekanos M, Mollazade M, Balistreri G, Amor R, Cooper-White JJ, Goodhill GJ, Meunier FA (2017) Visualizing endocytic recycling and trafficking in live neurons by subdiffractional tracking of internalized molecules. Nat Protoc 12:2590–2622.

Kaempf N, Kochlamazashvili G, Puchkov D, Maritzen T, Bajjalieh SM, Kononenko NL, Haucke V (2015) Overlapping functions of stonin 2 and SV2 in sorting of the calcium sensor synaptotagmin 1 to synaptic vesicles. Proc Natl Acad Sci USA 112:7297–7302.

Kechkar A, Nair D, Heilemann M, Choquet D, Sibarita JB (2013) Real-time analysis and visualization for single-molecule based super-resolution microscopy. PLoS One 8:e62918.

Kelly BT, Owen DJ (2011) Endocytic sorting of transmembrane protein cargo. Curr Opin Cell Biol 23:404–412.

Kononenko NL, Diril MK, Puchkov D, Kintscher M, Koo SJ, Pfuhl G, Winter Y, Wienisch M, Klingauf J, Breustedt J, Schmitz D, Maritzen T, Haucke V (2013) Compromised fidelity of endocytic synaptic vesicle protein sorting in the absence of stonin 2. Proc Natl Acad Sci USA 110: E526–E535.

Koo SJ, Markovic S, Puchkov D, Mahrenholz CC, Beceren-Braun F, Maritzen T, Dernedde J, Volkmer R, Oschkinat H, Haucke V (2011) SNARE motif-mediated sorting of synaptobrevin by the endocytic adaptors clathrin assembly lymphoid myeloid leukemia (CALM) and AP180 at synapses. Proc Natl Acad Sci USA 108:13540–13545.

Koo SJ, Kochlamazashvili G, Rost B, Puchkov D, Gimber N, Lehmann M, Tadeus G, Schmoranzer J, Rosenmund C, Haucke V, Maritzen T (2015) Vesicular synaptobrevin/VAMP2 levels guarded by AP180 control efficient neurotransmission. Neuron 88:330–344.

Lynch BA, Lambeng N, Nocka K, Kensel-Hammes P, Bajjalieh SM, Matagne A, Fuks B (2004) The synaptic vesicle protein SV2A is the binding site for the antiepileptic drug levetiracetam. Proc Natl Acad Sci USA 101:9861–9866.

Mendoza-Torreblanca JG, Vanoye-Carlo A, Phillips-Farfán BV, Carmona-Aparicio L, Gómez-Lira G (2013) Synaptic vesicle protein 2A: basic facts and role in synaptic function. Eur J Neurosci 38:3529–3539.

Nair D, Hosy E, Petersen JD, Constals A, Giannone G, Choquet D, Sibarita JB (2013) Super-resolution imaging reveals that AMPA receptors inside synapses are dynamically organized in nanodomains regulated by PSD95. J Neurosci 33:13204–13224.

Pan PY, Marrs J, Ryan TA (2015) Vesicular glutamate transporter 1 orchestrates recruitment of other synaptic vesicle cargo proteins during synaptic vesicle recycling. J Biol Chem 290:22593–22601.

Pyle RA, Schivell AE, Hidaka H, Bajjalieh SM (2000) Phosphorylation of synaptic vesicle protein 2 modulates binding to synaptotagmin. J Biol Chem 275:17195–17200.

Schindelin J, Arganda-Carreras I, Frise E, Kaynig V, Longair M, Pietzsch T, Preibisch S, Rueden C, Saalfeld S, Schmid B, Tinevez JY, White DJ, Hartenstein V, Eliceiri K, Tomancak P, Cardona A (2012) Fiji: an open-source platform for biological-image analysis. Nat Methods 9:676–682.

Schivell AE, Batchelor RH, Bajjalieh SM (1996) Isoform-specific, calcium-regulated interaction of the synaptic vesicle proteins SV2 and synaptotagmin. J Biol Chem 271:27770–27775.

Schivell AE, Mochida S, Kensel-Hammes P, Custer KL, Bajjalieh SM (2005) SV2A and SV2C contain a unique synaptotagmin-binding site. Mol Cell Neurosci 29:56–64.

Serajee FJ, Huq AM (2015) Homozygous mutation in synaptic vesicle glycoprotein 2A gene results in intractable epilepsy, involuntary movements, microcephaly, and developmental and growth retardation. Pediatr Neurol 52:642–646.

Tokudome K, Okumura T, Terada R, Shimizu S, Kunisawa N, Mashimo T, Serikawa T, Sasa M, Ohno Y (2016a) A missense mutation of the gene encoding synaptic vesicle glycoprotein 2A (SV2A) confers seizure susceptibility by disrupting amygdalar synaptic GABA release. Front Pharmacol 7:210.

Tokudome K, Okumura T, Shimizu S, Mashimo T, Takizawa A, Serikawa T, Terada R, Ishihara S, Kunisawa N, Sasa M, Ohno Y (2016b) Synaptic vesicle glycoprotein 2A (SV2A) regulates kindling epileptogenesis via GABAergic neurotransmission. Sci Rep 6:27420.

van Vliet EA, Aronica E, Redeker S, Boer K, Gorter JA (2009) Decreased expression of synaptic vesicle protein 2A, the binding site for levetiracetam, during epileptogenesis and chronic epilepsy. Epilepsia 50:422–433.

Wang D, Zhou Q, Ren L, Lin Y, Gao L, Du J, Wang Y (2019) Levetiracetam-induced a new seizure type in a girl with a novel SV2A gene mutation. Clin Neurol Neurosurg 181:64–66.

Yao J, Bajjalieh SM (2008) Synaptic vesicle protein 2 binds adenine nucleotides. J Biol Chem 283:20628–20634.

Yao J, Nowack A, Kensel-Hammes P, Gardner RG, Bajjalieh SM (2010) Cotrafficking of SV2 and synaptotagmin at the synapse. J Neurosci 30:5569–5578.

Zhang N, Gordon SL, Fritsch MJ, Esoof N, Campbell DG, Gourlay R, Velupillai S, Macartney T, Peggie M, van Aalten DM, Cousin MA, Alessi DR (2015) Phosphorylation of synaptic vesicle protein 2A at Thr84 by casein kinase 1 family kinases controls the specific retrieval of synaptotagmin-1. J Neurosci 35:2492–2507.